LAWRENCE
LIVERMORE
NATIONAL
LABORATORY

LLNL-JRNL-719499

Autoignition of binary blends of n-dodecane/1-methylnaphthalene andiso-cetane/1-methylnaphthalene

G. Kukkadapu, C. J. Sung

January 24, 2017

Autoignition of binary blends of
n-dodecane/1-methylnaphthalene and
iso-cetane/1-methylnaphthalene

Disclaimer

Autoignition of binary blends of *n*-dodecane/1-methylnaphthalene and *iso*-cetane/1-methylnaphthalene

Goutham Kukkadapu[a,b*], Chih-Jen Sung[b]

[a]Lawrence Livermore National Laboratory, Livermore, CA 94551, USA

[b]Department of Mechanical Engineering, University of Connecticut, Storrs, CT 06269, USA

Keywords: autoignition, *n*-dodecane, *iso*-cetane, 1-methylnaphthalene, diesel surrogates, rapid compression machine

Corresponding Author:
Goutham Kukkadapu
Lawrence Livermore National Laboratory
7000 East Avenue
Livermore, CA 94551, USA
E-Mail: kukkadapu1@llnl.gov
Phone: (925) 422-1489

Submitted for publication in Combustion and Flame

Revised: July 22, 2017

Manuscript Reference Number: CNF-D-17-00086R1

LLNL-JRNL-719499

Autoignition study of binary blends of *n*-dodecane/1-methylnaphthalene and *iso*-cetane/1-methylnaphthalene

Goutham Kukkadapu[a,b*], Chih-Jen Sung[b]

[a]Lawrence Livermore National Laboratory, Livermore, CA 94551, USA

[b]Department of Mechanical Engineering, University of Connecticut, Storrs, CT 06269 USA

Abstract

An experimental study on autoignition of two binary blends, *n*-dodecane/1-methylnaphthalene and *iso*-cetane/1-methylnaphthalene, has been conducted using a rapid compression machine. Specifically, the ignition delays of the stoichiometric blend+air mixtures were measured at elevated pressures of P_C=15 bar and 30 bar, compressed temperatures of T_C=626−944 K, and varying blending ratios of the constituents. For a given set of P_C and T_C, a nonlinear response of the blend reactivity with respect to the relative amount of the constituents was observed. Since a comprehensive chemical kinetic model for the blends investigated here is under development, the current ignition delay datasets serve as the needed targets for model validation. For selected conditions, ignition delay simulations were conducted to highlight and discuss the deficiencies of the literature models and the potential areas for model improvements, especially at low temperatures. Further chemical kinetic analyses were conducted to gain understanding of the blending behavior predicted by the available model.

LLNL-JRNL-719499

1. Introduction

Petroleum derived transportation fuels are complex mixtures of hydrocarbons, exhibiting diversity in the molecular classes, structures, and chain lengths. The composition diversity in the transportation fuels makes the development of their chemical kinetic models, which are needed for understanding the fundamental combustion processes and the engine performances related to ignition, extinction, emissions, etc., extremely challenging. One popular way to model the combustion kinetics of complex transportation fuels is the use of a simpler mixture of hydrocarbons, also termed "surrogate fuel", which mimics the physical or/and chemical properties of the target real fuel. These surrogate fuels are made up of a limited number of hydrocarbons that are representatives of the molecular classes, structures, and chain lengths found in the transportation fuels. Since the chemical kinetic models of surrogate fuels are typically assembled by merging the individual models of the constituent hydrocarbons, the ability of the surrogate models to capture the combustion characteristics of the target real fuels is reliant on the fidelity of the chemical kinetic models of the surrogate constituents. Besides accurately describing the combustion kinetics of the neat surrogate constituents, it is also necessary to capture the chemical kinetic interactions when the surrogate constituents are blended together. The primary objective of the current study is to investigate the ignition behaviors of various binary blends of the surrogate constituents relevant to diesel fuels.

The binary blends of the present interest are the fuel mixtures of 1-methylnaphthalene and *iso*-cetane (2,2,4,4,6,8,8 heptamethylnonane), as well as 1-methylnaphthalene and *n*-dodecane, at varying blending ratios. *n*-Dodecane, *iso*-cetane, and 1-methylnaphthalene have been chosen in this investigation as the representatives of *n*-alkanes, *iso*-alkanes, and aromatics, respectively, which constitute the major compound classes in diesel fuels [1]. In addition, 1-methylnaphthalene

and *iso*-cetane were chosen because they have been widely used in surrogate formulations [e.g., 2-5] and they are the reference fuels used for determining the cetane rating of a fuel. The choice of *n*-dodecane as the representative of *n*-alkanes, instead of *n*-cetane, was due to its relatively lower boiling point so that it is comparatively easier to handle in experiments. It is further noted that *n*-cetane and *n*-dodecane are homologous hydrocarbons, and hence they are expected to exhibit analogous oxidation chemistry and similar ignition characteristics.

Survey of the literature showed that while the chemical kinetics for the neat components of 1-methylnaphthalene [6-10], *iso*-cetane [11-14], and *n*-dodecane [15-24] have been studied experimentally to some detail, there are only very few studies on the binary blends involving these fuel components [9,25,26]. Wang *et al.* [9] studied the ignition of stoichiometric binary blends of *n*-decane/1-methylnaphthalene in air behind reflected shock waves at nominal pressures of 10 bar and 40 bar over a temperature range of 848−1349 K. Won *et al.* [25] measured the reflected shock ignition delays of a stoichiometric *iso*-cetane/*n*-cetane blend (54.1/45.9 in molar %) at a nominal pressure of 20 atm over a temperature range of 685−1250 K. Agosta *et al.* [26] studied the oxidation of the blends of *iso*-cetane/*n*-dodecane (60/40 in molar %) and 1-methylnaphthalene/*n*-dodecane (49/51 in molar %) in a flow reactor at a pressure of 8 atm and a residence time of 120 ms over a temperature range of 600−900 K.

Recognizing the need for more experimental studies on fuel blends, we have conducted elevated-pressure experiments using a rapid compression machine to investigate the autoignition characteristics of the binary blends of *n*-dodecane/1-methylnaphthalene and *iso*-cetane/1-methylnaphthalene with varying blending ratios. These new datasets from the current study shall provide insights into the blending behaviors and serve as high fidelity ignition delay data greatly sought for validating and refining the surrogate models under development. Further details of the

blend compositions, the experimental procedure, and the test conditions shall be specified and described in the next section. Later sections shall discuss the experimental data followed by the comparison with the simulated results using the chemical kinetic models available in the literature. Finally, the deficiencies of the literature models and the potential areas to refine them shall be identified and discussed.

2. Experimental specifications

2.1 Test mixtures

Tables 1 and 2 summarize the compositions of different fuel blend/O_2/N_2 mixtures and the molar % (X) of the components in the test mixtures investigated in the current study. From here on, *n*-dodecane, *iso*-cetane, and 1-methylnaphthalene shall be referred as *n*-C12, *i*-C16, and 1-MN, respectively. The oxidizer used here was the mixture of O_2 and N_2 in the molar proportion of O_2:N_2=1:3.76, while the stoichiometric condition was maintained for all test mixtures. Moreover, the values of "% *n*-C12 in the blend" and "% *i*-C16 in the blend" listed in Tables 1 and 2, respectively, correspond to the molar percentages of *n*-C12 and *i*-C16 in the respective binary fuel blends. Here, a wide range of varying proportions of the constituent hydrocarbons in the fuel blend was covered to investigate the response of the blend reactivity to the blending ratio. It is also noted from Tables 1 and 2 that the molar percentages of O_2 and N_2 in the test mixtures, X_{O2} and X_{N2}, remain largely unchanged as the equivalence ratio and the oxidizer composition were held fixed.

In addition, the derived cetane number (DCN) of each binary fuel blend is listed in Tables 1 and 2. The DCNs of the binary fuel blends were calculated using a linear relationship on a liquid volume basis, between the limits defined by values for the pure components, as given in [27]. It is seen from Tables 1 and 2 that a wide range of DCNs was also covered in this study.

Table 1: Molar compositions of test mixtures and DCNs of *n*-C12/1-MN blends.

$X_{n\text{-}C12}$ (%)	$X_{1\text{-}MN}$ (%)	X_{O2} (%)	X_{N2} (%)	molar % of *n*-C12 in the blend	DCN
1.12	0.00	20.77	78.11	100	87.0
0.85	0.37	20.75	78.03	70	68.6
0.57	0.76	20.73	77.94	43	47.0
0.41	0.97	20.72	77.90	30	35.3
0.22	1.23	20.70	77.85	15	20.0
0.15	1.33	20.70	77.82	10	13.1
0.08	1.43	20.69	77.80	5	6.7
0	1.53	20.69	77.78	0	0

Table 2: Molar compositions of test mixtures and DCNs of *i*-C16/1-MN blends.

$X_{i\text{-}C16}$ (%)	$X_{1\text{-}MN}$ (%)	X_{O2} (%)	X_{N2} (%)	molar % of *i*-C16 in the blend	DCN
0.85	0.00	20.83	78.32	100	15.1
0.72	0.24	20.81	78.23	75	12.9
0.55	0.55	20.78	78.12	50	10.0
0.32	0.96	20.74	77.98	25	2.7
0	1.53	20.69	77.78	0	0

2.2 Experimental procedure and test conditions

The rapid compression machine (RCM) at the University of Connecticut employs a creviced piston to compress test mixtures to elevated pressures and temperatures. The creviced piston is driven pneumatically and brought to rest towards the end of the compression stroke using a hydraulic pin-groove mechanism. While the compression time generally varies between 30 and 45 ms, the majority of pressure/temperature rise occurs in the last 6 ms of compression. A trigger from LabView® initiates the compression event and starts the subsequent data acquisition. The dynamic pressure in the reaction cylinder is measured using a thermal-shock resistant Kistler 6125C transducer in conjunction with a 5010B charge amplifier. The geometric compression ratio (CR) can be varied by changing either the stroke length or the clearance length at the end of compression

(EOC), as $CR = 1 + \frac{stroke\ length}{clearance\ length\ at\ EOC}$. The stroke length in the current design can be varied between 177.8 and 254 mm in an increment of 6.35 mm, while the clearance length at the EOC can be varied between 14 and 56 mm in an increment of 1 mm. By changing the clearance length at the EOC and stoke length, the operating geometric compression ratio can be varied from 4 to 20. The desired test condition at the end of compression, represented by compressed pressure (P_C) and compressed temperature (T_C), can be achieved by independently varying the geometric compression ratio, intake temperature (T_0), and intake pressure (P_0). Due to the heat transfer from hot gases to the wall during the compression stroke, the effective compression ratio achieved is generally lower than the geometric compression ratio. As the compressed temperature cannot be estimated directly using the geometric compression ratio, it is widely deduced using the measured pressure trace by applying the adiabatic core hypothesis:

$$\int_{T_0}^{T_c} \frac{\gamma}{\gamma - 1} \frac{\mathrm{d}T}{T} = \ln\left(\frac{P_c}{P_0}\right),$$

where γ is the specific heat ratio of the test mixture and is a function of temperature.

Prior to the start of an experiment, the reaction chamber is filled to the desired intake pressure with a homogenous fuel blend/oxidizer mixture prepared in a separate stainless steel mixing chamber. The mixing chamber, the RCM reaction chamber, and all the connecting manifolds are equipped with heaters to preheat the test mixture and the entire system uniformly to the desired intake temperature. The *n*-dodecane (>99% purity), *iso*-cetane (98% purity), and 1-methylnaphthalene (95% purity) used in the current study were obtained from Sigma-Aldrich®. The liquid fuels were injected into the mixing chamber on a mass basis using a glass syringe. The mass of the fuel injected into the mixing chamber was measured using an electronic mass balance with a least count of 0.01 gm. The oxidizer mixture was prepared by filling the mixing chamber

with constituent gases to the corresponding partial pressures manometrically. The mixing chamber, intake manifold, and reaction cylinder were heated to the desired preheat temperature for about 4 hours before starting the experiments. In addition, the mixing chamber is equipped with a magnetic stirrer that aids in preparation of homogeneous mixtures. Further details about the current RCM design and test procedure can be found in Das *et al.* [28].

Furthermore, because of the relatively high-boiling-point fuel components investigated here, the mixing chamber, intake manifold, and RCM were heated to a sufficiently high initial temperature to ensure that the partial pressures of the test fuel components were always less than their corresponding saturated vapor pressures at least by a factor of 1.5. In particular, an initial temperature of T_0=122 ^{o}C was used for experiments with the stoichiometric *n*-C12/air mixtures, while a preheat temperature of T_0=147 ^{o}C was used for all the other binary blends shown in Tables 1 and 2. Additionally, the intake pressures were varied in the range of 400–3000 Torr for the experiments conducted herein. The mixture preparation method used in the current study has been demonstrated previously [29] to yield homogenous fuel/oxidizer mixtures with negligible amount of fuel loss to adsorption and oxidation. In general, the uncertainty in mixture equivalence ratio is estimated to be about 5%. It is also noted that the ignition delays of neat 1-MN were taken from our recent work [10]. In the current RCM experiments, the test conditions covered the compressed pressures of P_C=15 bar and 30 bar, as well as the compressed temperatures of T_C=626−944 K.

Figure 1 shows the definitions of the first-stage ignition delay (τ_1) and the total ignition delay (τ) for reporting the present data, which were determined by the time differences between the EOC and the respective maxima of the time derivative of the pressure trace after the EOC. Using the experiments on the stoichiometric 15/85 *n*-C12/1-MN blend at P_C=15 bar and T_C=689 K as an example, Fig. 2 demonstrates the typical experimental repeatability of the data reported in the

current study. A minimum of four consecutive runs were conducted at each condition and the pressure trace closest to the mean of the measured results was used to determine the representative ignition delay value, as shown in Fig. 2. The scatter in ignition delays, both τ and τ_1, was less than 15% of the representative value for all the cases investigated here. Furthermore, to ensure repeatability, ignition delay data obtained from each fresh mixture was checked against that acquired from an earlier mixture.

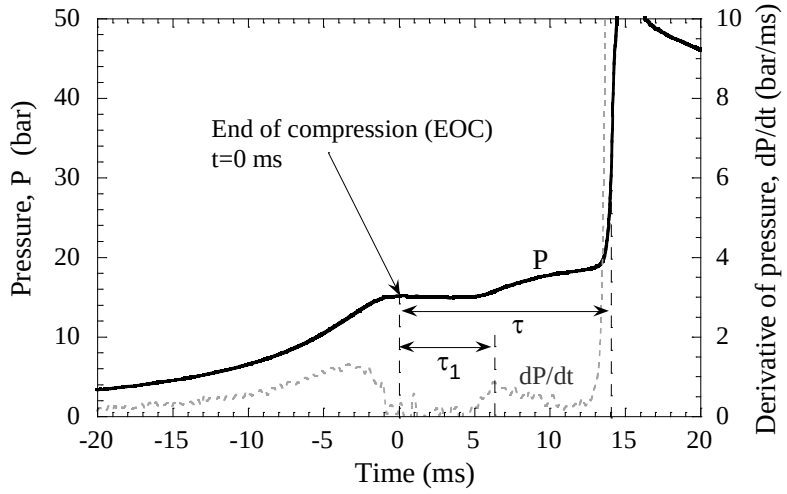

Figure 1. Plot showing the definitions of first-stage and total ignition delays used in this study.

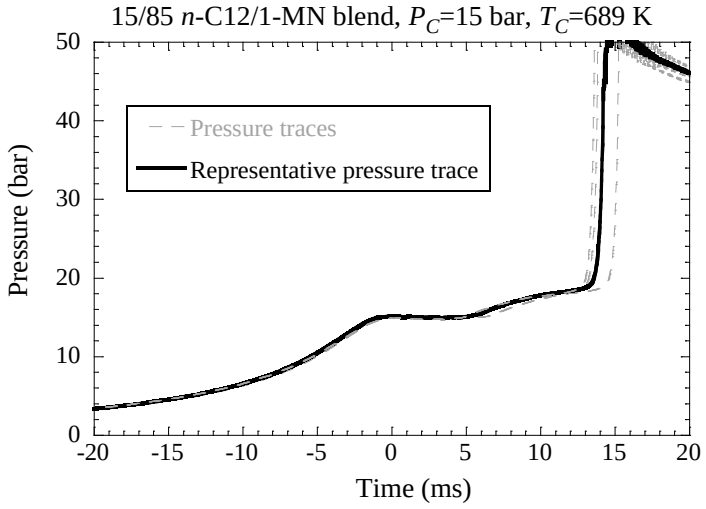

Figure 2. Plot showing the repeatability of the current data.

3. Experimental results

3.1 *n*-C12/1-MN binary blends

The ignition delay measurements of binary blends of *n*-C12/1-MN were conducted at a compressed pressure of P_C=15 bar over a wide compressed temperature range of T_C=655–936 K. At a nominal compressed temperature of T_C=669 K, Fig. 3(a) plots the experimental pressure traces at varying % *n*-C12 in the binary fuel blend. It can be seen from Fig. 3(a) that the pressure history appears to show a single-stage like ignition behavior when the % *n*-C12 exceeds 30%. For the blends containing less than 30% *n*-C12, two-stage ignition behavior is clearly observed in Fig. 3(a), with the pressure rise associated with the first stage of ignition increasing as the % *n*-C12 is raised. At proportions of *n*-C12 higher than 30%, the single-stage like ignition behavior could be a result of that the first stage reactivity becomes increasingly vigorous, and hence the transition to the second stage cannot be discerned in the pressure records.

Figures 3(b) and 3(c) respectively summarize the total and first stage ignition delays of the different *n*-C12/1-MN blends deduced from the pressure traces using the definitions shown in Fig. 1. The ignition delay measurements shown in Figs. 3(b) and 3(c) exclude those data points exhibiting exothermicity during the compression stroke. To identify the extent of exothermicity for each case, the pressure histories taken from the non-reactive counterparts, by replacing O_2 with N_2 in the test mixtures, were used as references. In addition, the ignition delays of the blends containing more than 10% *n*-C12 were limited to low temperatures, as further increase in compressed temperature resulted in exothermicity during the compression stroke. Figures 3(b) and 3(c) show that both the total ignition delays and the first stage ignition delays decrease with increasing amount of *n*-C12 in the blend. Furthermore, the negative temperature coefficient (NTC)

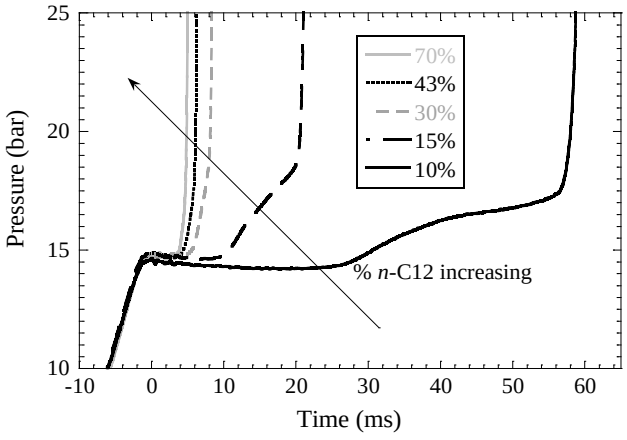

(a)

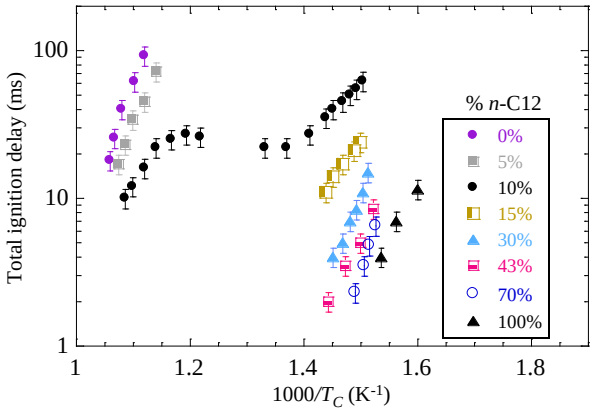

(b)

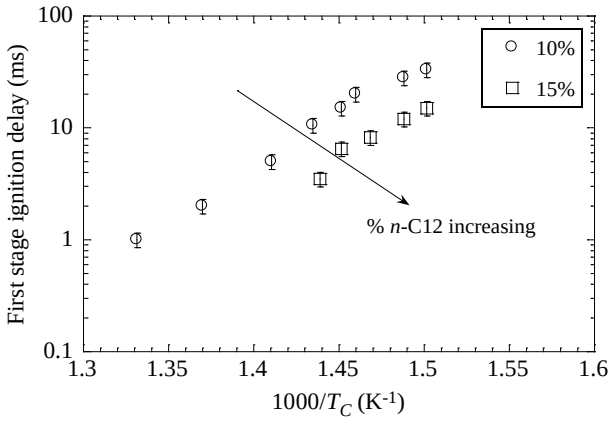

(c)

Figure 3: Plots showing (a) experimental pressure traces at compressed temperature of T_C=669±3 K, (b) total ignition delays, and (c) first stage ignition delays for *n*-C12/1-MN blends at varying blending ratios. The compressed pressure is P_C=15 bar.

characteristic is clearly seen in the total ignition delay results of the 10% *n*-C12 blend. Although the entire total ignition delay response curves of the other blends could not be resolved in the current RCM experiments as the onset of ignition was observed during the compression stroke, it is expected that blends with more than 10% *n*-C12 would also exhibit NTC characteristics in other circumstances.

To better understand the sensitivity of the total ignition delay variation with % *n*-C12 in the blend, the total ignition delays of the *n*-C12/1-MN blends at two different compressed temperatures were plotted and compared in Fig. 4. Figure 4 shows that the total ignition delay decreases nonlinearly with increasing % *n*-C12 in the blend. At T_C~893 K, the total ignition delays drop steeply upon small addition of *n*-C12 to the pure 1-MN case. Specifically, the total ignition delay decreases by a factor of about two when the % *n*-C12 in the blend increases from 0% to 5%. Further increase in % *n*-C12 from 5% to 10% shortens the total ignition delay by a factor of three. At a lower compressed temperature of T_C~669 K, Fig. 4 also illustrates that increasing % *n*-C12 in the blend continues to cause a steep drop in total ignition delays till the amount of *n*-C12 increases to 30%. Beyond that, namely increasing % *n*-C12 in the blends from 43% to 70%, the change in total ignition delay is less significant, reducing from ~5 ms to ~2.5 ms. Similar nonlinear dependence of total ignition delay on the constituent amount of binary blends was also noticed by Wang *et al.* [9] in their shock tube experiments with binary blends of *n*-decane/1-MN. The total ignition delay results shown in Fig. 4 demonstrate that when two fuel components with distinct reactivities are blended, small addition of the more reactive fuel (like *n*-C12 in the current case) to the less reactive fuel (like 1-MN) in large amount could result in a strong change in the global reactivity of the blend. On the other hand, small addition of the less reactive fuel to the more

reactive fuel of abundant presence may have weak or insignificant effect on the global reactivity of the blend.

Furthermore, using the experimental results of Fig. 4, the dependence of the total ignition delay on the DCN of the blend (cf. Table 1) is demonstrated in Fig. 5. It is seen that the measured total ignition delay decreases with increasing DCN and the experimental data can be correlated quite well with a dependence of $\tau \sim DCN^{-(1.725 \pm 0.175)}$.

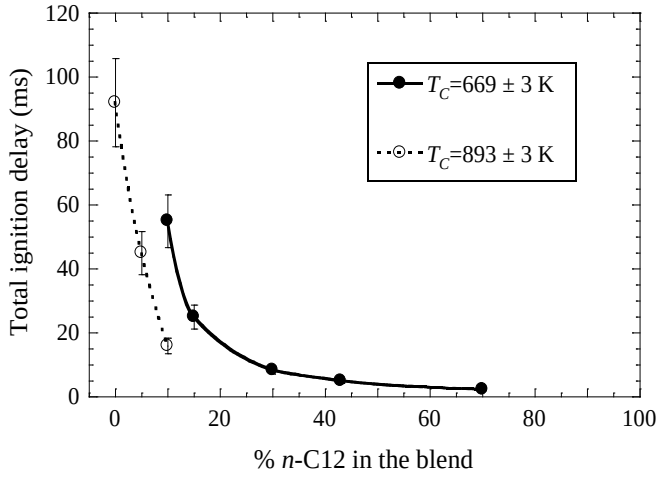

Figure 4: Plot showing the effect of % *n*-C12 in the *n*-C12/1-MN blends on total ignition delays at P_C=15 bar for two compressed temperatures of T_C~669 K and T_C~893 K.

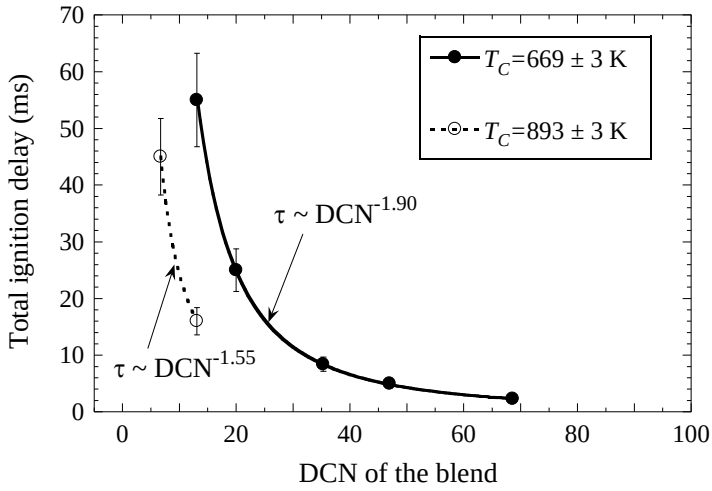

Figure 5. Plot showing the dependence of total ignition delay on DCN of the blend, based on the data of Fig. 4 at P_C=15 bar for two compressed temperatures of T_C~669 K and T_C~893 K.

1

LLNL-JRNL-719499

3.2 *i*-C16/1-MN binary blends

The ignition delay measurements of binary blends of *i*-C16/1-MN were conducted at two compressed pressures of P_C=15 bar and 30 bar. At P_C=15 bar, the *i*-C16/1-MN blends show no two-stage like behavior and no evidence of NTC is observed in Fig. 6(a) for the temperatures investigated in the current study. Figure 6(b) shows the experimental pressure traces of the stoichiometric 50/50 *i*-C16/1-MN blend at P_C=30 bar and three different compressed temperatures, in which two-stage ignition behavior is observed for compressed temperatures of 704 and 735 K. In addition, Fig. 6(b) shows that the pressure rise from the first stage ignition reduces as T_C increases from 704 K to 735 K. Further increasing T_C beyond 770 K, the pressure trace does not show any first stage ignition activity. The τ and τ_1 of the *i*-C16/1-MN blends at P_C=30 bar over a range of T_C are shown in Figs. 6(c) and 6(d), respectively. From the ignition delays shown in Fig. 6(c), it can be observed that the total ignition delays of the 50/50 *i*-C16/1-MN blend exhibit non-Arrhenius behavior at lower temperatures (T_C<770 K), which could be due to the underlying NTC chemistry and is supported by the two-stage ignition characteristics shown in Fig. 6(b) for pressure traces and in Fig. 6(d) for the first stage ignition delays. Figures 6(a) and 6(c) also illustrate that an increase in % *i*-C16 in the blend generally increases the reactivity of the system.

At two sets of P_C and T_C, namely 15 bar/893 K and 30 bar/858 K, Fig. 7 examines the response of total ignition delay to the amount of *i*-C16 in the *i*-C16/1-MN blends. The total ignition delays at both the compressed conditions decrease monotonically with increasing % *i*-C16. However, in the regime of small *i*-C16 addition (< 20%), the total ignition delay decreases more gradually with an increase in % *i*-C16. Figure 8 further shows the comparison of changes in total ignition delays due to the additions of *n*-C12 and *i*-C16 to 1-MN at P_C=15 bar and T_C ~893 K, demonstrating that the addition of *n*-C12 has a stronger promoting effect on reactivity. Since *n*-C12 is known to be

more reactive than *i*-C16, the observed difference in the ignition promoting effect can be attributed to the relative reactivities of these two alkanes.

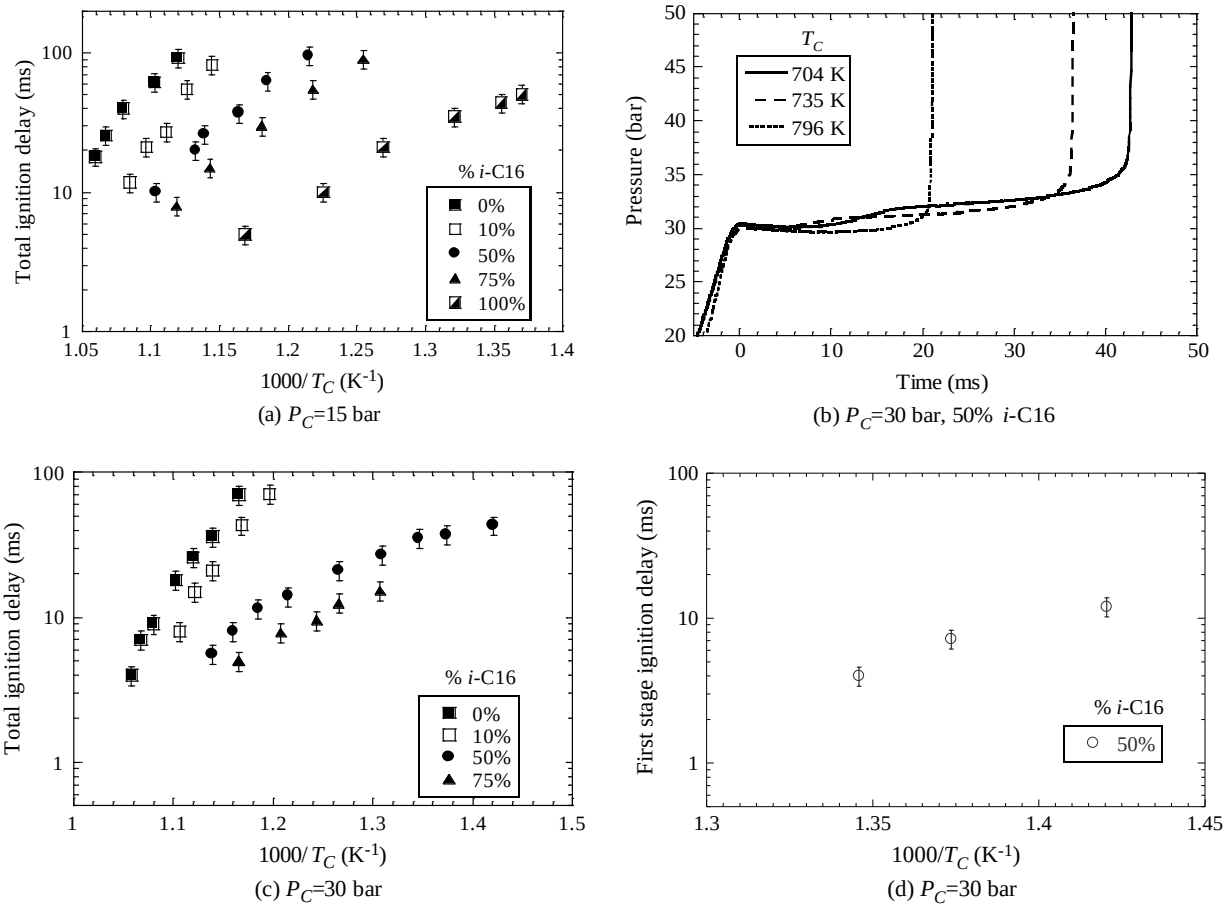

Figure 6: Plots showing (a) total ignition delays of *i*-C16/1-MN blends at P_C=15 bar, (b) experimental pressure traces of 50/50 *i*-C16/1-MN blend at P_C=30 bar and varying T_C, (c) total ignition delays of *i*-C16/1-MN blends at P_C=30 bar, and (d) first stage ignition delays of 50/50 *i*-C16/1-MN blend at P_C=30 bar.

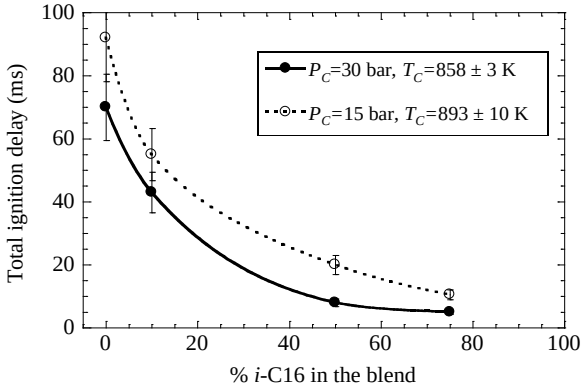

Figure 7: Plot showing total ignition delay variation with % *i*-C16 in the *i*-C16/1-MN blend.

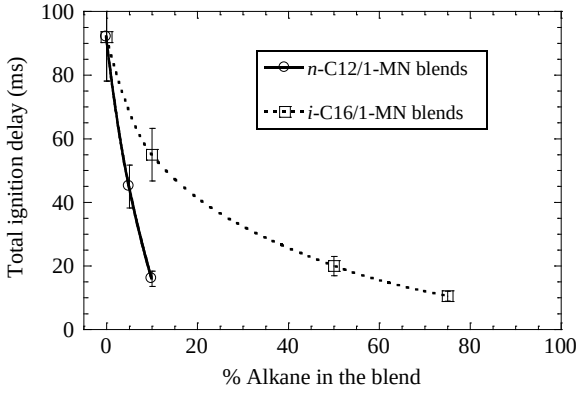

Figure 8: Plot showing total ignition delay variations with % *n*-C12 and % *i*-C16 in the blends, conducted at P_C=15 bar and T_C=893±10 K.

4. Kinetic analysis

4.1 *n*-C12/1-MN binary blends

From survey of the literature, we have identified several chemical kinetic models that describe the combustion chemistry of the three neat components [e.g., 9,11,30-32]. While the model of Narayanaswamy *et al.* [32] includes the kinetics of *n*-C12 and 1-MN, we could not identify a chemical kinetic model that describes the ignition chemistry of all the three hydrocarbons of interest in the current study. Hence, the simulated ignition delay results discussed in the following shall mainly focus on the *n*-C12/1-MN blends using the model of Narayanaswamy *et al.* [32]. Further reasons for not conducting ignition delay simulations for the *i*-C16/1-MN blends shall be discussed in the later section.

"Full RCM simulations" using the Chemkin-Pro package [33] were conducted here so that the physical and chemical processes prevalent in RCM experiments can be captured. In such simulations, the thermodynamic conditions are replicated using the associated volume history which includes both the compression phase and the post compression period, as show in Fig. 9. The volume history was modeled and deduced using the measured pressure trace of the

corresponding non-reactive experiment, along with the adiabatic core hypothesis. The non-reactive experiment was conducted by replacing O_2 with N_2 in the corresponding reactive mixture while keeping the same fuel concentration such that a similar specific heat ratio of the mixture is maintained and similar heat transfer characteristics exists between the reactive case and the non-reactive counterpart. The volume histories needed for simulating the current RCM experiments and the experimental pressure traces along with a summary of ignition delay measurements are available on our website at http://combdiaglab.engr.uconn.edu/database/rcm-database.

Figures 9(a) and 9(b) compare the experimental and simulated pressure traces for the 10/90 and 5/95 *n*-C12/1-MN blends. The former case exhibits a two-stage ignition behavior, while a single-stage ignition response is observed for the latter. As a reference, the corresponding non-reactive pressure trace is also plotted in Fig. 9, clearly showing the instant when significant reactivity commences and the extent of pre-ignition heat release. Using the chemical kinetic model of Narayanaswamy *et al.* [32], it is seen from Fig. 9 that the simulated results qualitatively capture the autoignition characteristics in general, but under-predict the experimental ignition delays and over-predict the first-stage pressure rise and the extent of pre-ignition heat release.

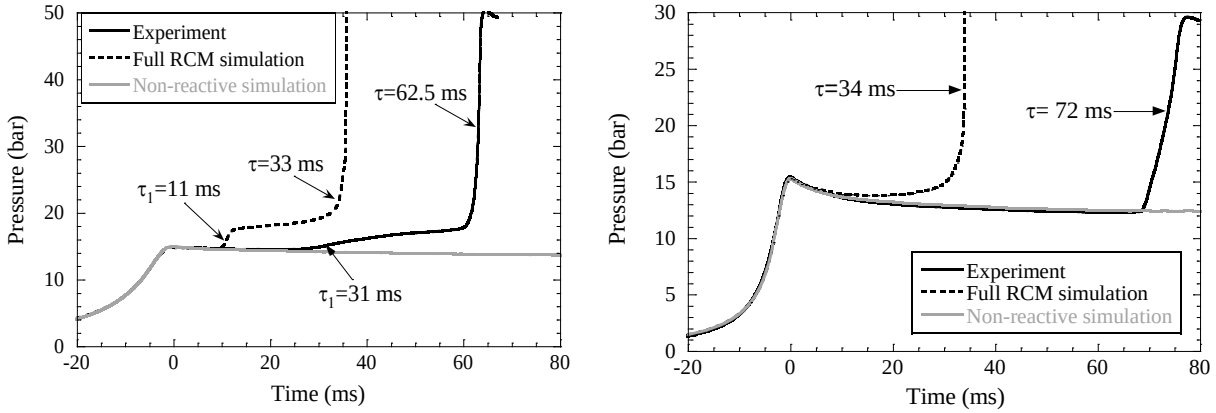

(a) P_C=15 bar, T_C=669 K, 10% *n*-C12, 90% 1-MN

(b) P_C=15 bar, T_C=880 K, 5% *n*-C12, 95% 1-MN

Figure 9: Plot showing the comparison of pressure traces from experiments and simulations for (a) 10/90 *n*-C12/1-MN blend and (b) 5/95 *n*-C12/1-MN blend.

Figure 10 shows the comparisons of the ignition delays of the pure components of *n*-C12 and 1-MN, as well as the different *n*-C12/1-MN blends, obtained from experiments and simulations. At P_C=15 bar, Fig. 10(a) displays that the simulated results using the sub-mechanism of *n*-C12 in the model of [32] are significantly less reactive than the current RCM data at low temperatures (T_C<700 K). Therefore, the discrepancies noticed at low temperatures illustrate that further improvements are necessary to the *n*-C12 sub-mechanism of [32]. Figure 10(b) compares the experimental and simulated total ignition delays of neat 1-MN at P_C=15 bar and 30 bar. The simulated results obtained using the 1-MN sub-mechanism of [32] appear to be more reactive than the RCM data at lower end of the compressed temperatures. It is also noted from Fig. 10(b) that the difference between experimental and simulated results decreases gradually with increasing T_C up to a compressed temperature where a crossover in reactivity is observed. Beyond the crossover point, the 1-MN sub-mechanism of [32] becomes less reactive than the current RCM experiments. Further discussion on the experimental and simulated results of 1-MN can be found in [10].

The total ignition delays of the *n*-C12/1-MN blends obtained from experiments and simulations are compared in Fig. 10(c) for P_C=15 bar. The performance of the model of [32] in estimating the total ignition delays of the binary blends does not show a consistent trend and is found to be dependent on the % *n*-C12 in the blend, which can be better understood from the total ignition delay comparison shown in Fig. 10(d) for T_C~669 K. Specifically, the simulated total ignition delay of the blend containing 70% *n*-C12 is seen to be about a factor of two greater than the experimental value, while the simulated results of the blends containing 15% and 30% *n*-C12 compare well against the experimental data with the differences being close to the experimental uncertainty. On the other hand, the simulated total ignition delay of the 10% *n*-C12 blend is a factor of 1.7 lower than the experimental value. For compressed temperatures greater than 730 K, since the RCM simulations for the blend containing 10% *n*-C12 exhibit ignition during the

compression stoke, those simulated results are not shown in Fig. 10(c). Furthermore, the comparison of the total ignition delays of the blend containing 5% *n*-C12 over a range of compressed temperatures from experiments and simulations shows trends similar to those observed in the pure 1-MN case of Fig. 10(b).

Figure 10(e) shows the comparison of the first stage ignition delays observed from simulations and experiments for the blends containing 10% and 15% *n*-C12. The first stage ignition delays predicted by the model are consistently shorter, with the simulated values being generally about a factor of two shorter than the experimental results. It is to be noted that the simulated total ignition delays of the 15% *n*-C12 blend are seen in Fig. 10(c) to match closely with the experimental data while the first stage ignition delays differ by a factor of two. To summarize, the model of Narayanaswamy *et al.* [32] qualitatively captures the ignition delay variations with % *n*-C12 in the blend, despite showing significant differences in the quantitative values.

As the model of Narayanaswamy *et al.* [32] is able to predict the blending characteristics qualitatively, further reaction path analysis was conducted to identify important reaction channels and understand the underlying chemistry responsible for blending behavior. Specifically, a constant-volume adiabatic simulation was carried out using the stoichiometric 10/90 *n*-C12/1-MN blend with an initial temperature of 670 K and an initial pressure of 15 bar, which is an experimental condition related to Fig. 4. The reaction path fluxes were computed at the time instant corresponding to 10% consumption of *n*-C12, at which the associated temperature rise is ~3 K, and the results are shown in Fig. 11.

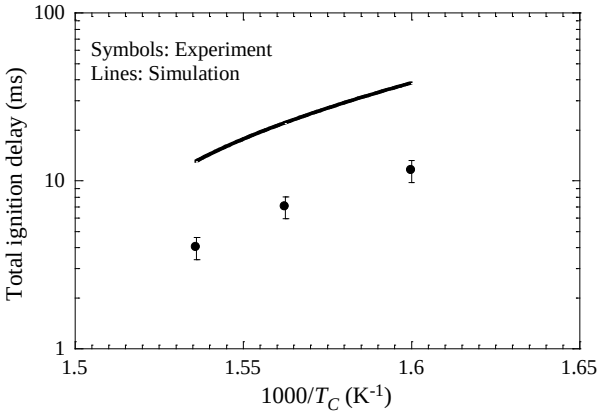

(a) 100 % *n*-C12, P_C=15 bar

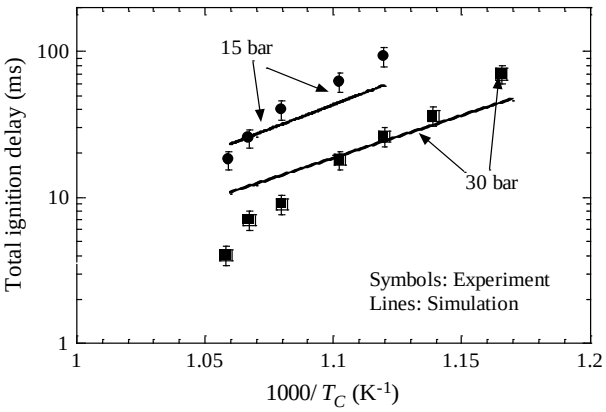

(b) 100% 1-MN

1

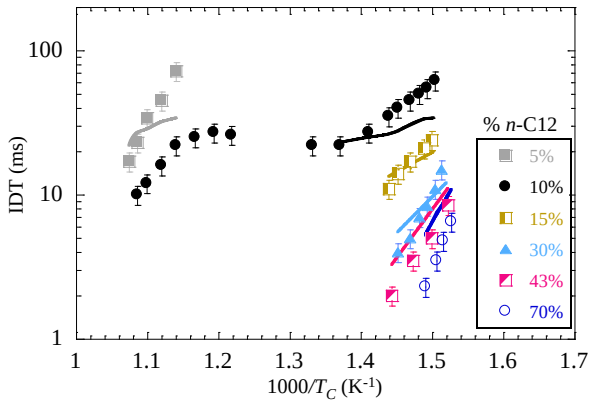

(c) *n*-C12/1-MN blends, P_C=15 bar

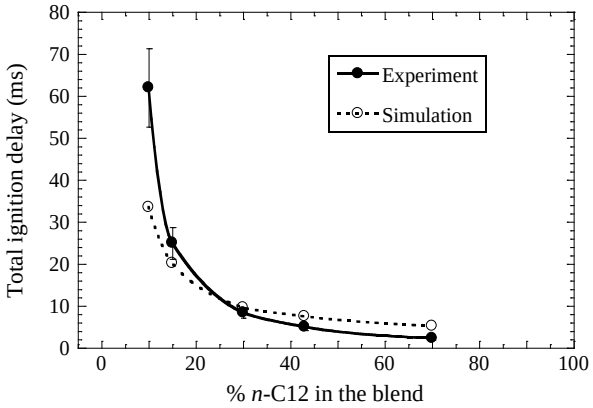

(d) P_C=15 bar, T_C=669±3 K

2

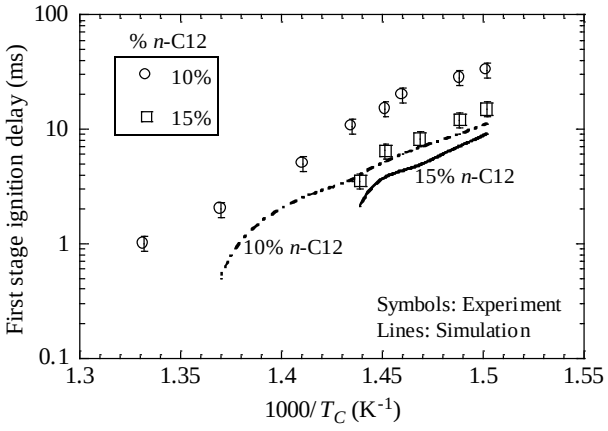

(e) *n*-C12/1-MN blends, P_C=15 bar

3

4 Figure 10: Comparisons of total ignition delays of (a) neat *n*-C12, (b) neat 1-MN, and (c) *n*-C12/1-
5 MN blends over a range of T_C, (d) total ignition delays of *n*-C12/1-MN blends at T_C~669 K, and
6 (e) first stage ignition delays of *n*-C12/1-MN blends from experiments and simulations using the
7 model of Narayanaswamy *et al.* [32].
8

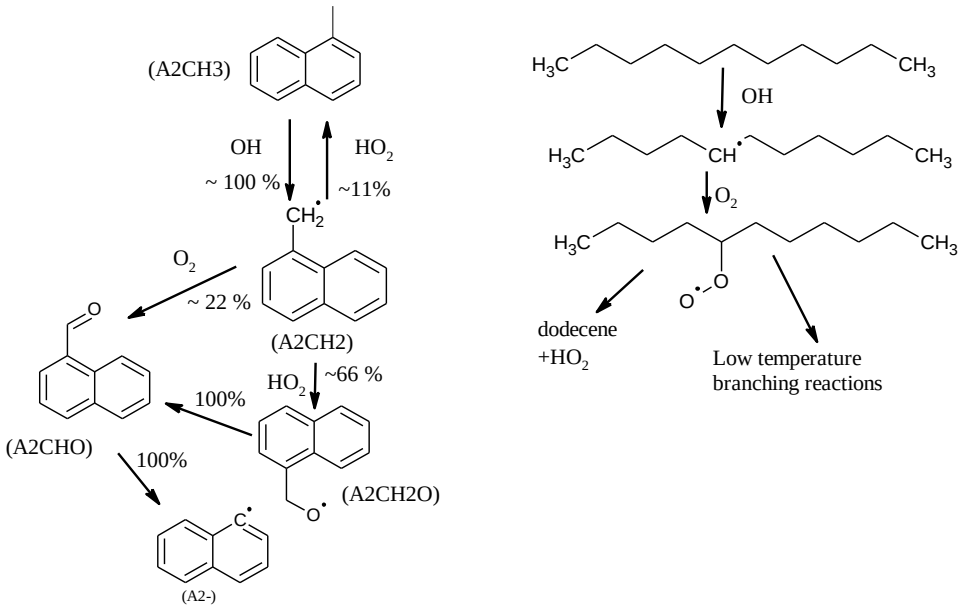

Figure 11: Reaction flux analysis showing the important consumption pathways of 1-MN and *n*-C12 in the 10/90 *n*-C12/1-MN blend at the time instant corresponding to 10% consumption of *n*-C12. Constant-volume adiabatic simulation was conducted with an initial temperature of 670 K and an initial pressure of 15 bar.

Figure 11 show that both *n*-C12 and 1-MN are predominantly consumed by the H-abstraction reactions via OH, leading to *n*-dodecyl (C12H25) and 1-methylnaphthyl (A2CH2) radicals, respectively. It is to be noted that in the current model of [32], the six possible *n*-dodecyl radicals are lumped to one radical species, C12H25. The *n*-dodecyl radicals produced from the H-abstraction reactions are subsequently consumed by the addition reactions with molecular oxygen (O_2) leading to formation of peroxy adduct, thus initiating the low temperature chain branching reactions. Very small amount (<10%) of the dodecyl peroxy radicals produced undergo the concerted elimination reactions producing *n*-dodecene (lumped species) and hydroperoxyl radical (HO_2). Further, the 1-naphthylmethyl (A2CH2) radicals are consumed by the reactions with O_2 and HO_2 producing 1-naphthaldehyde (A2CHO) and 1-methylnaphthoxyl (A2CH2O) radicals, respectively, along with OH. The 1-methylnaphthoxyl (A2CH2O) radicals subsequently undergo unimolecular decomposition to produce 1-naphthaldehyde (A2CHO) and H radicals. In addition,

the unimolecular decomposition of A2CH2O is the predominant (>90%) source of H in the system. As the H radicals are consumed by the association reactions with O_2 to produce HO_2, this association reaction is the primary source (>90%) of HO_2 radicals in the system. The HO_2 radicals are predominantly (>90%) consumed by the reactions with 1-naphthylmethyl (A2CH2) radicals at these temperatures regenerating the OH radicals.

Since the current model of Narayanaswamy *et al.* [32] does not include any cross reactions, the blending behavior shown in Fig. 11 is mainly attributed to the competition between *n*-C12 and 1-MN in consuming the major radicals such as OH and HO_2 for the temperatures of interest in the current study. To elucidate this, a rate of production analysis of OH was further conducted to compare the consumption of the OH radicals by *n*-C12 and 1-MN at different blending ratios, based on constant-volume adiabatic simulations with an initial temperature of 670 K and an initial pressure of 15 bar. As done in Fig. 11, the relative OH consumption between *n*-C12 and 1-MN for a given blend was determined at the time instant corresponding to 10% consumption of *n*-C12. At this particular time instant, the OH consumption ratio is defined by the following equation:

$$\text{OH consumption ratio} = \frac{\sum_{i=1}^{M} \dot{\omega}_{(OH+1MN)i}}{\sum_{i=1}^{N} \dot{\omega}_{(OH+nC12)i}}.$$

Here, $\dot{\omega}_{(OH+1MN)i}$ is the consumption rate of OH by reaction *i* involving both OH and 1-MN and *M* is the total number of such reactions. Similarly, $\dot{\omega}_{(OH+nC12)i}$ is the consumption rate of OH by reaction *i* involving both OH and *n*-C12 and *N* is the total number of such reactions. Based on the current definition, the OH consumption ratio provides the information about the consumption of the OH radicals by 1-MN relative to that by *n*-C12. Figure 12 shows the calculated OH consumption ratios at varying % *n*-C12 in the blend. It is seen from Fig. 12 that the ratio of OH consumption exhibits a nonlinear behavior which is similar to the characteristic behavior of the

experimental total ignition delays, also shown in Fig. 12. The similarity between the OH consumption ratio and the total ignition delay response (or blend reactivity) can be explained by the relative efficacies of the low temperature chemistry of the resultant fuel radicals produced from the abstraction reactions. The *n*-dodecyl radicals produced from the H-abstraction reactions of *n*-dodecane would facilitate a highly degenerate chain branching reaction scheme typical to *n*-alkanes which accelerates ignition event, while the abstraction reactions from the benzylic site in 1-MN initiate a low temperature reaction scheme which is well known to be weaker than that of *n*-alkanes, and hence retard ignition. From the trend shown in Fig. 12, it can be inferred that for blends with low amounts of *n*-C12 (e.g., 5% and 10%) the performance of the model is mainly controlled by the ignition chemistry of 1-MN, while the performance of the model at high amounts of *n*-C12 is controlled predominantly by the performance of the *n*-C12 submodel. Therefore, the discrepancies observed in the simulated and experimental ignition delays of binary blends (cf. Fig. 10) can be primarily attributed to the efficacy of the model performance against the ignition delays of pure components of 1-MN and *n*-C12.

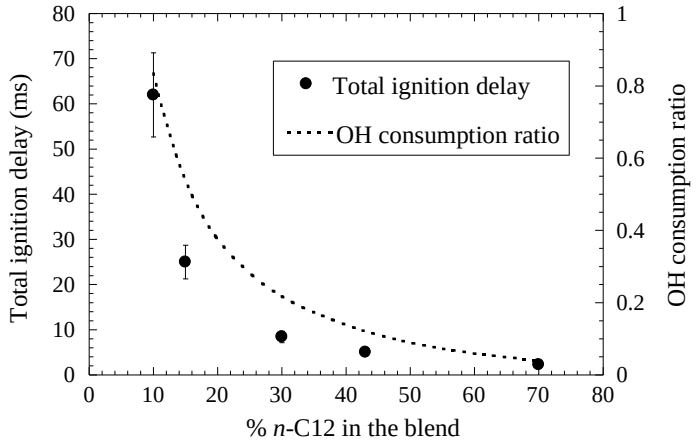

Figure 12: Plot illustrating the ratio of OH consumption by 1-MN relative to that by *n*-C12 at varying amounts of *n*-C12 in the blend. Constant-volume adiabatic simulations were conducted with an initial temperature of 670 K and an initial pressure of 15 bar. The OH consumption was calculated at the time instant corresponding to 10% consumption of *n*-C12 for a given blend.

4.2 *i*-C16/1-MN binary blends

Using the model of Oehlschlaeger *et al.* [11], Fig. 13 compares the experimental and simulated total ignition delays of stoichiometric *i*-C16/air mixtures at P_C=15 bar. As seen from Fig. 13, the model of [11] is more reactive than experiments for T_C<815 K and the discrepancy increases with decreasing T_C. Besides the differences in total ignition delays, the pressure traces from simulations show a two-stage like ignition in the compressed temperature range investigated, which, however, was not observed in the RCM experiments. It has to be pointed out that the model of [11] was developed based on the *iso*-octane model of Curran *et al.* [34] and to our knowledge it has never been validated against the experimental data of *i*-C16 at low temperatures. Modifications to the chemical kinetic models of various *n*- and *iso*-alkanes developed on the basis of the models of Curran *et al.* [34,35] have recently been proposed to improve their predictive nature [36-39], and hence similar modifications might be necessary to improve the fidelity of the *i*-C16 model of [11]. Considering the poor performance of the *i*-C16 model available in the literature, further ignition delay simulations of the current *i*-C16/1-MN blends were not conducted.

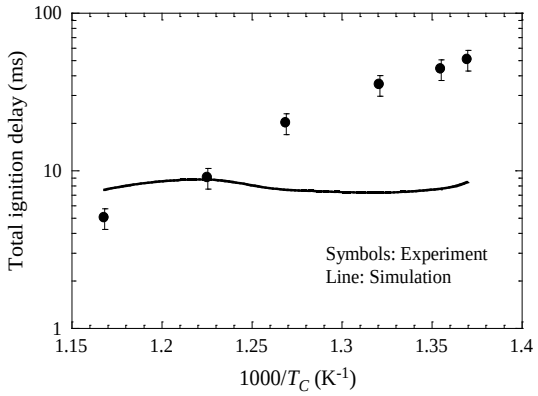

Figure 13: Comparison of total ignition delays from experiments and simulations for neat *i*-C16 at P_C=15 bar. Simulations were conducted using the model of Oehlschlaeger *et al.* [11].

Comparisons shown in Figs. 10 and 13 illustrate several differences observed between experiments and simulations and highlight the needs for refining the chemical kinetic models of *i*-C16, *n*-C12, 1-MN, and their blends. A recent study on autoignition of 1-MN [10] has identified and discussed several potential changes that may need to be incorporated into the model of Narayanaswamy *et al.* [32] to improve its fidelity. The suggested changes for the 1-MN model include addition of missing pathways and use of appropriate rates for some of the important reactions [10]. In addition, the possible modifications needed to improve the fidelity of the models of *i*-C16 and *n*-C12 include re-evaluating the thermodynamic properties of the important species, addition of missing reaction pathways, and updating the reaction rate rules of various reaction classes as done by the studies of [36-39]. Cai *et al.* [40] have recently proposed an optimized kinetic model of C_7–C_{12} *n*-alkanes which includes the updates to the reaction rate rules and the thermodynamic properties of the important species. Figure 13 shows the performance of the Cai *et al.* model [40] in estimating the total ignition delays of neat *n*-C12 measured in the current study. As seen in the Fig. 14, the model of Cai *et al.* [40] performs much better than the earlier model of Narayanaswamy *et al.* [32], and hence suggests that the performance of *i*-C16 and *n*-C12 models could be improved by re-evaluating the thermodynamic properties of the important species, including missing reaction pathways, and updating the reaction rate rules. Refining the models of *i*-C16, *n*-C12, and 1-MN would require comprehensive chemical kinetic studies which are beyond the scope of the current study, and for the same reason further chemical kinetic analyses were not conducted here.

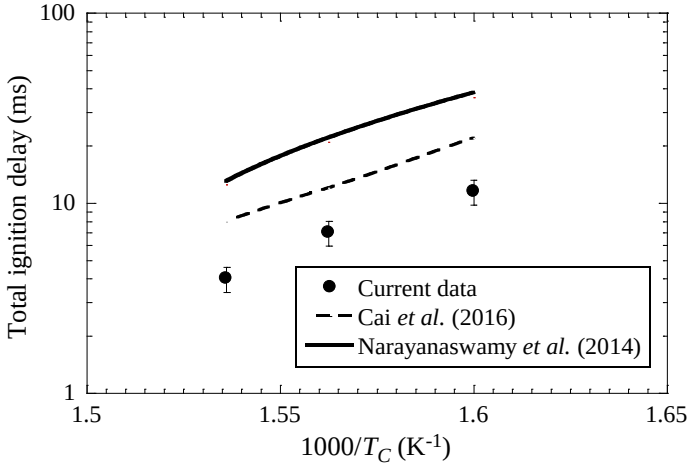

Figure 14: Plot showing the comparison of the total ignition delays for stoichiometric *n*-C12/air mixtures obtained from the current RCM experiments and the simulations using two literature kinetic models of [32,40].

5. Conclusions

Ignition delay measurements of the binary blends of *n*-C12/1-MN and *i*-C16/1-MN were conducted using a rapid compression machine. Experiments were conducted with stoichiometric blend/air mixtures at elevated pressures of P_C=15 bar and 30 bar and over a compressed temperature range of T_C=626–944 K. For a given set of P_C and T_C, the experimental results showed that an increase in % *n*-C12 in the *n*-C12/1-MN blend resulted in a nonlinear decrease in the total ignition delay with a steep drop when small amounts of *n*-C12 were added. An increase of % *i*-C16 in the *i*-C16/1-MN blend was also found to cause a nonlinear decrease in total ignition delays, but the drop in the small *i*-C16 addition regime was not as steep.

Ignition delay simulations were further conducted to assess the performances of the chemical kinetic models available in the literature. Significant discrepancies were noted between the experimental and simulated ignition delays of the binary blends of *n*-C12/1-MN when using the model of Narayanaswamy *et al.* [32], while this model was seen to capture the qualitative trends observed in experiments. Even for the neat components of *n*-C12 and 1-MN, the comparison of

the present RCM data and the simulated results using the model of [32] shows significant differences at low temperatures. Chemical kinetic analyses were also conducted to gain insights into the blending behavior predicted by the model of [32]. For the simulations of the neat *i*-C16 experiments, the model of Oehlschlaeger *et al.* [11] was found to be significantly more reactive than the present RCM experiments at low temperatures, with the discrepancy increases with decreasing compressed temperature. The results from the current study show that the *n*-C12/1-MN model of [32] and the *i*-C16 model of [11] need further improvement at low temperatures.

Acknowledgements

The work at UCONN was supported by the National Science Foundation under Grant No. CBET-1402231. GK was supported by the U.S. Department of Energy (DOE), Office of Energy Efficiency and Renewable Energy (EERE), Solar Energy Technologies Office (SETO) under contract no. DE-AC52-07NA27344 through the Special Employee Strategic Mission Support Program and also by the Lawrence Livermore National Laboratory via Standard Research Subcontract No. B617843.

References

1. R. Gieleciak, C. Fairbridge, Detailed hydrocarbon analysis of FACE diesels using comprehensive two-dimensional gas chromatography. http://www.crcao.org/publications/advancedVehiclesFuelsLubricants/FACE/GCxGC%20analysis%20of%20FACE%20fuels%20-RG%20v4%200%20Nov2013.pdf.
2. J. T. Farrell, N. P. Cernansky, F. L. Dryer, D. G. Friend, C. A. Hergart, C. K. Law, R. M. Mc David, C. J. Mueller, A. K. Patel, H. Pitsch, Development of an experimental database and kinetic models for surrogate diesel fuels, SAE International, 2007-01-0201, 2007.
3. C. J. Mueller, W. J. Cannella, T. J. Bruno, B. Bunting, H. D. Dettman, J. A. Franz, M. L. Huber, M. Natarajan, W. J. Pitz, M. A. Ratcliff, K. Wright, Methodology for formulating diesel surrogate fuels with accurate compositional, ignition quality and volatility characteristics, Energy Fuels, 26 (2012), pp. 3284–3303.
4. K. Anand, Y. Ra, R. D. Reitz, B. Bunting, Surrogate model development for fuels for advanced combustion engines, Energy Fuels, 25 (2011), pp. 1474–1484.
5. C. V. Naik, K. Puduppakkam, E. Meeks, Simulation and analysis of in-cylinder soot formation in a low temperature combustion diesel engine using a detailed reaction mechanism, 2013-01-1565, Apr. 2013., SAE Int. J. Engines, 6(2) (2013), pp. 1190–1201.
6. C. B. Shaddix, K. Brezinsky, I. Glassman, Oxidation of 1-methylnaphthalene, Proc. Combust. Inst., 24 (1992), pp. 683–690.
7. C. B. Shaddix, K. Brezinsky, I. Glassman, Analysis of fuel decay routes in the high-temperature oxidation of 1-methylnaphthalene**,** Combust. Flame, 108 (1997), pp. 139–157.
8. U. Pfahl, K. Fieweger, G. Adomeit, Self-ignition of diesel-relevant hydrocarbon-air mixtures under engine conditions, 26th International Symposium on Combustion, 1996, pp. 781-789.

9. H. Wang, S. J. Warner, M. A. Oehlschlaeger, R. Bounaceur, J. Biet, P. A. Glaude, F. Battin-Leclerc, An experimental and kinetic modeling study of the autoignition of α-methylnaphthalene/air and α-methylnaphthalene/n-decane/air mixtures at elevated pressures Combust. Flame, 157 (2010), pp. 1976-1988.
10. G. Kukkadapu, C. J. Sung, Autoignition study of 1-methylnaphthalene in a rapid compression machine, Energy Fuels, 31 (1) (2017), pp. 854-866.
11. M. A. Oehlschlaeger, J. Steinberg, C. K. Westbrook, W. J. Pitz, The autoignition of iso-cetane at high to moderate temperatures and elevated pressures: shock tube experiments and kinetic modeling, Combust. Flame, 156 (2009), pp. 2165-2172.
12. S. H. Won, F. M. Haas, A. Tekawade, G. Kosiba, M. A. Oehlschaleger, S. Dooley, F. L. Dryer, Combustion characteristics of C_4 iso-alkane oligomers: experimental characterization of iso-dodecane as a jet fuel surrogate component, Combust. Flame, 165 (2016), pp. 137-143.
13. P. Dagaut., K. Hadj-Ali, Chemical kinetic study of the oxidation of iso-cetane in a jet stirred reactor: experimental and modeling, Energy Fuels, 23 (2009), pp. 2389-2395.
14. B. Li, H. Zhang, F. N. Egolfopoulos, Laminar flame propagation of atmospheric iso-cetane/air and decalin/air mixtures, Combust. Flame, 161 (2014), pp. 154-161.
15. S. S. Vasu, D. F. Davidson, Z. Hong, V. Vasudevan, R. K. Hanson, n-Dodecane oxidation at high-pressures, Measurement of ignition delay times and OH concentration time-histories, Proc. Combust. Inst., 32 (2009), pp. 173-180.
16. M. S. Kurman, R. H. Natelson, N. P. Cernansky, D. L. Miller, Speciation of the reaction intermediates from n-dodecane oxidation in the low temperature regime, Proc. Combust. Inst., 33 (2011), pp. 159-166.

17. A. Mze-Ahmed, K. Hadj-Ali, P. Dagaut, G. Dayma, Experimental and modeling study of the oxidation kinetics of n-undecane and n-dodecane in a jet-stirred reactor, Energy Fuels, 26 (2012), pp. 4253-4268.
18. H. S. Shen, J. Steinberg, J. Vanderover, M. A. Oehlschaleger, A shock tube study of the ignition of *n*-heptane, *n*-decane, *n*-dodecane, and *n*-tetradecane at elevated pressures, Energy Fuels, 23 (2009), pp. 2482-2489.
19. X. Hui, C. J. Sung, Laminar flames speeds of transportation-relevant hydrocarbons and jet fuels at elevated temperatures and pressures, Fuel, 109 (2013), pp. 191–200.
20. C. Ji, E. Dames, Y. L. Wang, H. Wang, F. N. Egolfopoulos, Propagation and extinction of premixed C_5 to C_{12} n-alkane flames, Combust. Flame, 157 (2010), pp. 277–287.
21. K. Kumar, C. J. Sung, Laminar flame speeds and extinction limits of preheated n-decane/O_2/N_2 and n-dodecane/O_2/N_2 mixtures, Combust. Flame, 151 (2007), pp. 209–224.
22. T. Malewicki, K. Brezinsky, Experimental and modeling study on the pyrolysis and oxidation of n-decane and n-dodecane, Proc. Combust. Inst., 34 (2013), pp. 361–368.
23. D. F. Davidson, D. R. Haylett, R. K. Hanson, Development of an aerosol shock tube for kinetic studies of low-vapor-pressure fuels, Combust. Flame, 155 (2008), pp. 108–117.
24. D. F. Davidson, Z. Hong, G. L. Pilla, A. Farooq, R. D. Cook, R. K. Hanson, Multi-species time history measurements during n-dodecane oxidation behind reflected shock waves, Proc. Combust. Inst., 33 (2011), pp. 151–157.
25. S. H. Won, S. Dooley, P. S. Veloo, H. Wang, M. A. Oehlschlaeger, F. L. Dryer, Y. Ju, The combustion properties of 2,6,10 trimethyldodecane, a chemical function group analysis, Combust. Flame, 161 (2014), pp. 826-834.

26. A. Agosta, N. P. Cernansky, D. L. Miller, T. Faravelli, E. Ranzi, Reference components of jet fuels: kinetic modeling and experimental results, Exp. Therm. Fluid Sci., 28 (2004), pp. 701–708.
27. J. Yanowitz, M. A. Ratcliff, R. L. McCormick, J. D. Taylor, Compendium of experimental cetane numbers, http://www.nrel.gov/docs/fy14osti/61693.pdf.
28. A. K. Das, C. J. Sung, Y. Zhang, G. Mittal, Ignition delay study of moist hydrogen/oxidizer mixtures using a rapid compression machine, Int. J. Hydrogen Energy, 37 (2012), pp. 6901–6911.
29. K. Kumar, G. Mittal, C. J. Sung, Autoignition of n-decane under elevated pressure and low-to-intermediate temperature conditions, Combust. Flame, 156 (2009), pp. 1278-1288.
30. S. M. Sarathy, C. K. Westbrook, M. Mehl, W. J. Pitz, C. Togbe, P. Dagaut, H. Wang, M. A. Oehlschlaeger, U. Niemann, K. Seshadri, P. S. Veloo, C. Ji, F. N. Egolfopoulos, T. Lu, Comprehensive chemical kinetic modeling of the oxidation of 2-methylalkanes from C_7 to C_{20}, Combust. Flame, 158 (2011), pp. 2338-2357.
31. K. Narayanaswamy, G. Blanquart, H. Pitsch, A consistent chemical mechanism for the oxidation of substituted aromatic species, Combust. Flame, 157 (2010), pp. 1879-1898.
32. K. Narayanaswamy, P. Pepiot, H. Pitsch, A chemical mechanism for low to high temperature oxidation of n-dodecane as a component of transportation fuel surrogates, Combust. Flame, 161 (2014), pp. 866-884.
33. CHEMKIN-PRO. San Diego: Reaction Design; 2013.
34. H. J. Curran, P. Gaffuri, W. J. Pitz, C. K. Westbrook, A comprehensive modeling study of iso-octane oxidation, Combust. Flame, 129 (2002), pp. 253-280.

35. H. J. Curran, P. Gaffuri, W. J. Pitz, C. K. Westbrook, A comprehensive modeling study of n-heptane oxidation, Combust. Flame, 114 (1998), pp. 149-177.
36. J. Bugler, B. Marks, O. Mathieu, R. Archuleta, A. Camou, C. Grégoire, K. A. Heufer, E. L. Petersen, H. J. Curran, An ignition delay time and chemical kinetic modeling study of the pentane isomers, Combust. Flame, 163 (2016), pp. 138-156.
37. K. Zhang, C. Banyon, C. Togb, P. Dagaut, J. Bugler, H. J. Curran, An experimental and kinetic modeling study of n-hexane oxidation, Combust. Flame, 162 (2015), pp. 4194-4207.
38. S. Y. Mohamed, L. Cai, F. Khaled, C. Banyon, Z. Wang, M. J. Al Rashidi, H. Pitsch, H. J. Curran, A. Farooq, S. M. Sarathy, Modeling ignition of a heptane isomer: improved thermodynamics, reaction pathways, kinetics, and rate rule optimizations for 2-methylhexane, J. Phys. Chem. A, 120 (2016), pp. 2201–2217.
39. N. Atef, G. Kukkadapu, S. Y. Mohamed, M. Al Rashidi, C. Banyon, M. Mehl, A. Heufer, E. F. Nasir, A. Alfazazi, A. K. Das, C. K. Westbrook, W. J. Pitz, A. Farooq, C. J. Sung, H. J. Curran, S. M. Sarathy, Comprehensive chemical kinetic modeling of *iso*-octane combustion with improved thermochemistry and kinetics, Combustion and Flame, 178 (2017), pp. 111-134.
40. L. Cai, H, Pitsch, S. Y. Mohamed, V. Raman, Bugler, H. J. Curran, S. M. Sarathy, Optimized reaction mechanism rate rules for ignition of normal alkanes, Combustion and Flame, 173 (2016), pp. 468-482.